Additive Manufacturing 33 (2020) 101111

Contents lists available at ScienceDirect

Additive Manufacturing

journal homepage: www.elsevier.com/locate/addma

Full Length Article

Design of a low-cost, high-temperature inverted build environment to enable desktop-scale additive manufacturing of performance polymers

Callie Zawaski, Christopher Williams*

Virginia Tech, 413E Goodwin Hall, Blacksburg, VA, 24061, United States

ARTICLE INFO

Keywords:
Material extrusion
Fused filament fabrication
High-performance polymers
Heated build chamber

ABSTRACT

A heated build environment in Fused Filament Fabrication (FFF) additive manufacturing (AM) is used to promote layer bonding in printed parts and reduce the difference in temperature between the extrusion and environment decreasing the shrinkage, residual stresses, and part deformation. A build environment capable of maintaining a high-temperature (> 200 °C) is often required to enable high-quality FFF printing of high-glass-transition, high-performance polymers such as nylon, PPSF, and ULTEM. Industrial-scale AM systems are capable of printing such polymers, as they offer a controlled, high-temperature printing environment; however, the machine cost often exceeds > $100,000. High-temperature printers are now available and at lower costs; however, the cost is still expensive (~$30,000). Many of these printers use bed heating rather than controlled environment heating, which can lead to inhomogeneous heat transfer and inconsistent properties. The key barrier to offering high-temperature environments for desktop-scale FFF systems in a cost-effective manner is that the electrical components must be compatible with, protected from, or removed from environments exceeding 100 °C.

To enable desktop-scale FFF printing of high-performance polymers at a low cost and high quality, the authors present a novel inverted FFF system design that provides a build environment of up to 400 °C. The inverted configuration effectively isolates the system electronics from the heated build environment, which allows for the use of inexpensive components. In this paper, the authors verify the inverted design concept analytically via a computational fluid dynamics model. The concept is then experimentally validated via a comparison of the strength of PPSF components printed on the inverted desktop-scale FFF system.

1. High temperature fused filament fabrication

1.1. Introduction

Fused Filament Fabrication (FFF), a type of material extrusion additive manufacturing (AM) technology, has the largest market install base of all AM systems [1]. FFF has been used for the fabrication of functional prototypes, tooling, and end-use parts in industrial (e.g., automotive, aerospace, medical), educational, and hobbyist markets. The small size, and inexpensive desktop FFF machines effectively democratize manufacturing by providing users access to AM with low barrier to entry. Furthermore, the commodity thermoplastic materials used in FFF create accurate parts with robust mechanical properties, which enables broad application.

Recently, the materials available for desktop FFF have been expanding from ABS and PLA to include other materials such as polyethylene terephthalate glycol (PETG) [2], thermoplastic polyurethane (TPU) [3], polyvinyl alcohol (PVA) [4], polycaprolactone (PCL) [5], and a variety of filled variants [6–8]. High performance materials, including ULTEM, polyether ether ketone (PEEK), and polyphenylsulfone (PPSF or PPSU) are also available; however, they are currently only printable on expensive, industrial-scale FFF systems. Such high-performance polymers have higher processing temperatures (e.g. > 300 °C) and require higher FFF nozzle temperatures due to the materials' relatively high glass transition temperature (T_g). They also require a high temperature heated environment to reduce part curling [9,10], and to increase overall part strength [11,12]. Part curling occurs when printing a thermoplastic when a hot layer is deposited on and bonded to a cold layer, where it then cools and shrinks. The shrinking of the bonded layer creates internal stresses within the part that can cause the previous layers to either curl or delaminate [13,14]. A heated environmental chamber reduces this effect by limiting the difference in the environment and extrusion temperature, and therefore the amount of shrinkage that occurs [15].

* Corresponding author.
E-mail address: cbwill@vt.edu (C. Williams).

https://doi.org/10.1016/j.addma.2020.101111
Received 22 October 2019; Received in revised form 31 January 2020; Accepted 4 February 2020
Available online 13 February 2020

Additionally, a heated chamber also has been shown to improve the part strength. Manufacturing the part in a heated environment decreases the rate of cooling of an extruded substrate, which increases the weld time promoting chain diffusion and increased entanglement between layers to generate a stronger weld [19,20]. For example, printing PEEK in a high temperature environment results in a stronger part, with a higher percent crystallinity [11]. PEEK printed in an ambient temperature of 200 °C demonstrated an improved of about 40 % in the tensile strength and elastic modulus compared to PEEK parts printed in room temperature. There are other techniques that also address the part strength by pre-heating the deposited strand using a laser [16], microwave [17], or heating element [18]. However, for materials that have a high thermal expansion, pre-heat treating the previous layer still creates a large thermal gradient in the part, which will result in curling. A heated environment improves both the layer bonding and reduces part curling.

1.2. Review of existing high-temperature environment machines

High temperature FFF is enabled via specialized machines that print parts within a high-temperature environment. In addition to Stratasys' Fortus line of printers, new systems have arrived recently in the market with the ability to print PEEK, polyetherimide (PEI), polyvinylidene fluoride (PVDF), acetal copolymer (POM-C), and nylon (PA6,6, and PA6,12). These systems have increasing cost with capable printing temperatures (Fig. 1).

The maximum temperature of the machine is effectively limited by the system's component with the lowest operating temperature range. These parts and components with extended operating temperature ranges increase the total cost of the printer, which effectively limits access to these high-performance polymers. Fig. 1 lists existing commercially available high-temperature 3D printers and their advertised maximum steady state temperatures. From this synthesis, it is observed that the maximum temperature of the machine has a roughly logarithmic relationship with the cost of the printer.

To avoid intellectual property conflicts [15], most of the high temperature machines rely on conduction of the heat through the bottom of the print bed to minimize curling. The bed is limited to maintaining temperatures below the T_g of the polymer to prevent deformation of a part's bottom layers. In their patent regarding the use of heated build chamber in FFF, Stratasys reports the ideal environment temperature being between the material's solidification temperature and its creep relaxation temperature [15]. This means printing tall parts on a heated bed (no heated environment), the top of the part is too far removed from the heat source and cannot gain all of the layer bonding benefits of the additional heating. Furthermore, complex-shaped parts may experience uneven heating/cooling throughout the part.

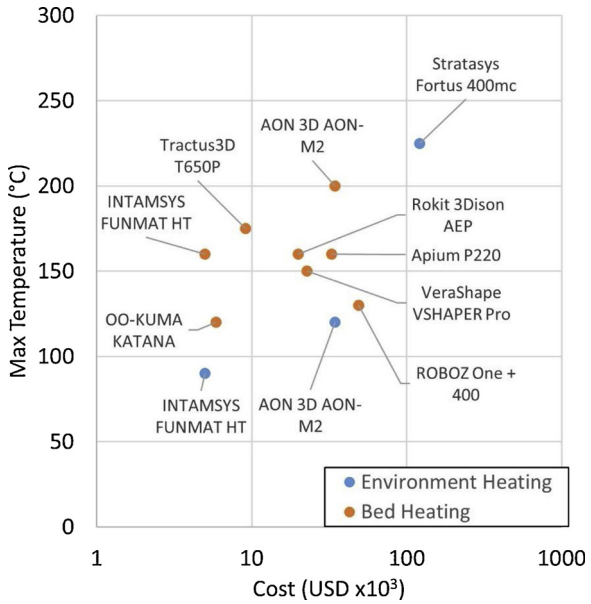

Fig. 1. The advertised maximum temperature for and cost for FFF systems featuring bed and/or environment heating [21–30].

A heated chamber is a more stable design solution as it maintains the printing environment to a uniform, elevated temperature. The steady uniform temperature brings the entire part closer to T_g, which creates stronger bonds between part layers due to the higher bonding potential [12], as well as decreasing the residual internal stresses.

Yang's prior research on printing PEEK suggests that an ambient temperature of at least 200 °C is sufficient for printing parts with high mechanical properties [11]. Most of the available printers shown in Fig. 1 are incapable of such high temperatures and the printers that can are very expensive.

1.3. Objective

Given this observed gap in FFF performance and cost, the authors aim to realize a FFF system that can print high-performance polymers at a low cost. The authors introduce a novel FFF system design that (1) exceeds current high-temperature systems to enable the capability of printing new high-performance materials and (2) can be applied to desktop-scale FFF machines. Specifically, the authors explore an inverted heated build chamber which uses natural convection to maintain a high temperature environment without exposing standard electronics to these temperatures.

Design considerations are first evaluated in Section 2.1, and their design tradeoffs are shown in Section 2.2. The core design tradeoff is maintaining a high temperature environment while keeping low-cost (low-operating temperatue) electronics and used to inform the basis of the design solution (Section 3.1). The design concept was modeled using CFD to evaluate the heat transfer (Section 3.2) and validated (Section 4.2.1) by a prototype system. PPSF tensile specimens were printed to quantify the improvement in material strength; a complex part was also printed to demonstrate the ability to print different design features (Section 4.2.2).

2. Design problem of a heated-environment system

The design discussion begins with first highlighting the customer needs and the key design considerations for the system. The design considerations are then evaluated against each other and the design tradeoffs for different existing solutions are discussed.

2.1. Design considerations/customer needs

2.1.1. Environment temperature

The primary design requirement is to maintain steady environmental temperature of at least 200 °C. Yang et al.'s work informs that printing PEEK requires a minimum environment temperature of 200 °C to improve the part mechanical properties [11]. However the continuous development of new materials may require environment temperatures exceeding 200 °C. In order to not limit the solution to current existing materials, the environment temperature should be maximized.

2.1.2. Component temperature

When using high-temperature environments, whether it is environmentally controlled or controlled by a heated bed in an enclosure, special consideration needs to be taken for all of the exposed machine components (e.g., motors, wires (wire coating), belts, polymer mounts and brackets, etc.) that may be affected by the elevated temperatures. Parts can be affected by different failure modes when subjected to prolonged exposure to high operating temperatures. For example, typical low-cost stepper motors used in desktop-scale FFF systems (e.g., a

NAME17) to drive the XYZ gantry are limited to operating in temperatures below ~100 °C for any sustained period of time, as stepper motors magnets lose their magnetism at elevated temperatures.

When designing the heated environment, the exposure of all components within it needs to be considered. The placement of each component must allow for the component to operate within its designed stable operating temperature range without sacrificing printing functionality and performance.

2.1.3. Cost

For the solution to be suitable for the authors' goal of enabling democratization of 3D printing high-performance polymers, the total cost of the machine with high temperature environment capabilities needs to be minimized. The cost of each printed part is the combination of the cost of the material, machine, labor, and its operation and maintenance divided by the number of parts printed during the machine's lifetime [31]. Thus it is advantageous to design the high temperature build environment so that both the initial price of the machine is low, as well as the cost associated with operation and maintenance.

2.2. Discussion of design tradeoffs

The key design tradeoff is maintaining low-cost components despite the need for them to operate in and/or near high-temperatures. Fig. 2 contains three potential design solutions for the components' interaction with the heated environment. The components must be compatible with (Fig. 2a), protected from (Fig. 2b), or removed from (Fig. 2c) the high-temperature environment for the machine to function. All of the high temperature printers from Section 1.2 embody one or more of these solutions across different components used. Here the authors isolate these solutions and evaluate the tradeoffs.

2.2.1. Components compatible with the high-temperature environment

In this solution using "compatible components", only parts and electronics that are able to operate in the high-temperature environment for sustained periods of time are used. For example, a printer can be enclosed inside of an insulated chamber, such as the Afinia H800 (Afinia 3D). The Afinia uses heat from the print bed in order to heat the part and the environment. This solution is sufficient for commodity plastics such as ABS. The Afinia is not marketed for high-temperature polymers due to the low-cost plastics and electronics used in the machine that are not rated for temperatures greater than about 100 °C. Incorporating higher temperature rated electronics would allow for increased build environment temperatures; however, these components are typically more expensive and pose new limits that may or may not be sufficient for high-temperature polymers.

2.2.2. Components protected from high-temperature environment

"Protected components" are defined by adding insulation and/or cooling to protect components and electronics from the high-temperature environment. This has the advantage of expanding the operating range of components to be able to operate at a higher environment temperatures without replacing them. A patent exists on a design for actively cooling the printer electronics [32]. AON-M2 is one commercial machine that uses liquid-cooled hot end and motion components to allow an increased environment chamber temperature [22]. A non-commercial design that uses protected components is documented by NASA, for modifying an existing 3D Printer (Lulzbot Taz 4) for printing high-temperature polymers. This modification includes adding an enclosure around the printer, active cooling for the motors, added heat lamps at the print bed, and replacing plastic parts [33]. Using heat lamps is a different way of protecting the electronics by focusing heat to the printing parts, creating inconsistent heating in the environment, thus the air around the part is hotter, where it is needed, than the air around the motors, where it is not needed.

Protecting components allows for the increase in the environment temperature past the limitation of the motors and larger electronics. However, the build environment temperature is still limited by any belts, plastic parts, wire insulation, etc. that are more difficult to protect and must be replaced with compatible components.

2.2.3. Removed components

"Removed components" refers to removing all of the parts and electronics from being inside, or in contact with the high temperature needed for the environment. A patent that uses this design concept is owned and used by Stratasys for their FFF systems [10]. The motors are positioned externally to the heated chamber, using a linear screw and belts to move the bed and print head. This design concept has the advantage of isolating the machine components, and allowing the heated environment to exceed any component temperature limits.

The challenge with this design is thoroughly insulating the build chamber, excluding the extruder motor, while still allowing full

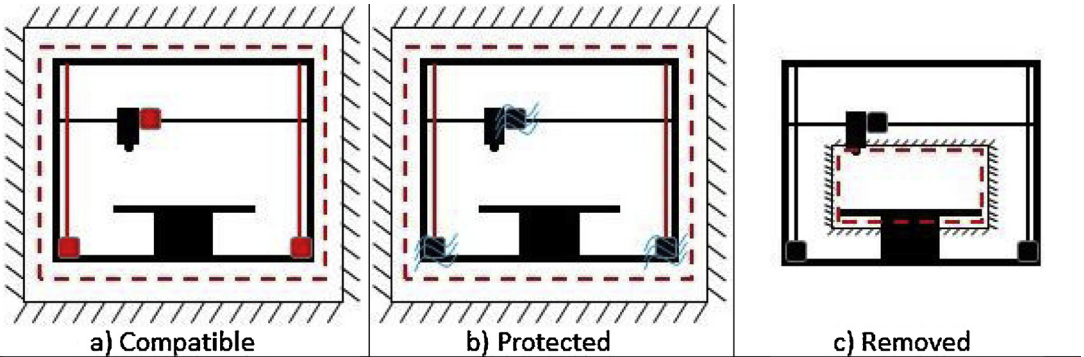

	a) Compatible	b) Protected	c) Removed
Pro	• Easy to implement • Enclosed heated environment	• Easy to implement • Allows for increased environment temperature	• Environment temperature not limited by components
Con	• Environment temperature is limited by electronic components	• Environment temperature is limited by components that cannot be protected • New failure risk	• More complex system required to insulate, while allowing movement, which results in heat loss

Fig. 2. Three design concepts for handling the components compatibility to enable printing in high temperature environments.

movement of the print head inside the build chamber. For example, the Fortus 400mc machine chamber top is insulated using a plastic accordion baffle to allow movement of the print head in the build space. The accordion insulation is insufficient to prevent heat from escaping into the top of the machine, which contains the print head components. The current designs that remove components have heat loss outside the chamber, resulting in some components being exposed to elevated temperatures.

3. Inverted printer design for a high-temperature build environment

3.1. Design

Removing the components from the heated environment is the only design solution that does not limit the temperature of the environment to the operating temperature of the components. This could allow for all printer components used for the motion and control of the printer to be inexpensive components that operate at room temperature. Such a solution would enable both minimizing the cost and maximizing the environment temperature. Removing the components still poses the design challenge of properly insulating the build environment for temperatures > 200 °C to minimize the energy loss, while allowing full movement of the print head within the chamber. High-temperature insulation typically uses glass and ceramic fibers to create a brittle cloth-like texture, which breaks and crumbles with excessive movement. The print head requires full movement within the build chamber and moves constantly while printing (at speeds more than 60 mm/s) for extended periods of time. The contradictory requirements between the print heads constant motion and the insulation breaking with movement poses a difficult design challenge.

At high temperatures, the most important wall of the build environment to insulate is the top of the build environment due to the natural, vertical flow of air as its temperature increases (and density decreases, as per Charles Law). Correspondingly, the bottom of the environment is less important to fully insulate, as it will experience less heat loss. Therefore, the authors argue that it would be advantageous to *invert the printer*, where insulation can easily be applied to the top and walls of the build chamber, and the bottom of the build chamber can remain open to allow for free movement of the print head.

A schematic of the proposed inverted high-temperature system is shown in Fig. 3. In the inverted configuration, the heated environment will act similar to a closed environment due to the difference in density of the cold and hot air, which will create a density barrier where the hot, less dense air will rise above the cool air. The inverted system effectively removes all printer components from the heated build environment, effectively solving the tradeoff between the cost of the component and the operating temperature discussed in Section 2.2. The feasibility of printing in an inverted configuration have been documented in previous research to verify the use of FFF for zero-G environments [34].

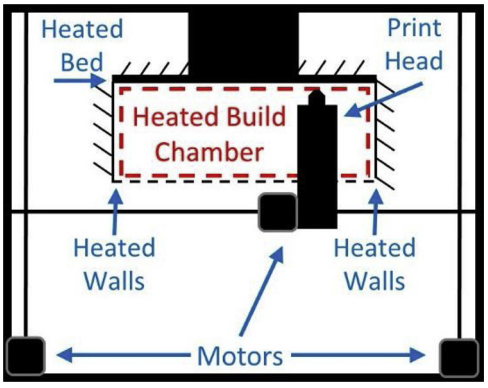

Fig. 3. High environment temperature system design, where the printer is inverted to allow for an open bottom to the heated print area for the print head to be able to access without inhibiting movement.

While this inverted design enables a high-temperature heated environment; however, it does impose some limitations to the process. For example, the inverted configuration may not be compatible with a hybrid AM system [35] or in-situ embedding of non-printed parts [36,37]. The technique or tool used in a hybrid design must also be compatible with the inverted configuration. For example, material jetting partially relies on gravity to dispense the material, and is therefore not compatible with the inverted design. An embedding system also has challenges with gravity with the addition that the embedded components must be compatible with the high-temperature environment for the duration of the print.

3.2. Verification via computational fluid dynamics model

To verify that a high-temperature environment could be reached and sustained with the inverted FFF concept, and that a temperature barrier would be created, the system was modeled using computational fluid dynamics (CFD). The model is used to evaluate the feasibility of the design and does not include the additional thermal mass of the part and the moving print head. A 2D steady state, pressure-based model was used, with a coupled pseudo-transient solution method in Ansys 17.0 Fluent. The chamber was modeled at 50.8 mm × 152.4 mm to match the dimensions of the physical prototype (Section 4). The walls were modeled as a 6.35 mm thick aluminum plate at a constant temperature of 200 °C. An open atmosphere around the opening of the chamber (304.8 mm × 304.8 mm) was defined to simulate the temperature where the system electronic components reside. Fig. 4a shows the simulation setup. Fluent does not have an open boundary condition, therefore an intake-fan was used to model the open boundary, with turbulence intensity of 5% and a turbulence viscosity ratio of 10. The sensitivity of the turbulence and other fluent boundary conditions were modeled to verify the assumed boundary condition did not significantly affect the temperature gradient or velocity profile within the chamber. The density, specific heat capacity, thermal conductivity, and viscosity of air were manually input as a piece-wise linear function of temperature. Sensitivity analysis was performed on the mesh and boundary conditions to ensure the accuracy of the model.

The resulting thermal map and velocity profile are shown in Fig. 4b and c. As hypothesized, trapped hot air rises to the top of the chamber which forms a temperature gradient at the boundary of the chamber and the open atmosphere. Heat generating from both the walls and the print bed create a vertical temperature profile with a horizontal temperature boundary and even heating throughout the environment. Air heated by the walls causes the air to flow upward along the wall, through natural convection. The vertical flow on the walls of the chamber then pushes the air on the top of the chamber to then flow inward and down creating a circular flow. Warm air recirculates as it nears the temperature boundary due to the lower density warm air remaining above the cool air to effectively enclose the warm air in the chamber. The temperature was maintained with 1% error for 4.4 mm z-height (> 198 °C), 5% error for 19.2 mm z-height (> 190 °C), and 10 % error for 29.8 mm z-height (> 180 °C), without including the heat provided by the print head or conduction through the part. This model shows how a consistent print chamber temperature of 200 °C can be created using an inverted chamber with heated walls and print bed.

To verify that the overall system design is generalizable for larger dimensions, the simulation was run with differently sized chambers (Fig. 5). This allows for a comparison of the 50.8 mm × 152.4 mm chamber (Fig. 5a) to a (2) taller (304.8 mm × 152.4 mm) (Fig. 5b), (3) wider (50.8 mm × 304.8 mm) (Fig. 5c), and (4) taller and wider (304.8 mm × 304.8 mm) (Fig. 5d) chamber. The results of these simulations are synthesized in Fig. 5 and demonstrates that increasing the

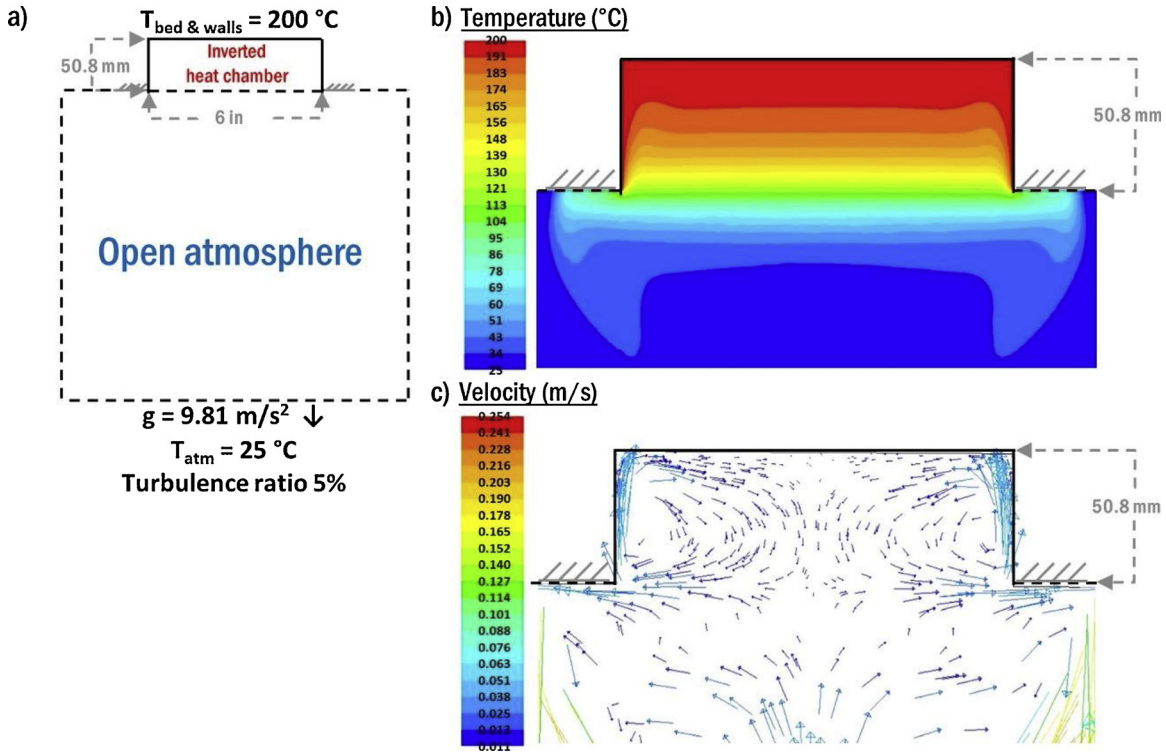

Fig. 4. The simulation output for the a) the experimental set up, b) temperature profile, and c) the velocity profile for the inverted heat chamber.

chamber depth results in the temperature gradient remaining at the boundary of the heated chamber. The chamber width does not significantly affect the temperature gradient boundary. Increasing the size of the chamber becomes physically challenging to build and produce an isothermal wall boundary condition; however, building a smaller isothermal wall for desktop scale systems is trivial. The thermal gradient remains consistently approximately 40 mm into the print chamber and 30 mm outside the print chamber boundary. The deeper chambers were able to maintain temperature for a larger volume, where the 304.8 mm × 152.4 mm chamber maintained 1% error for 240 mm z-height (> 198 °C), and 5% error for 270 mm z-height (> 190 °C). The 304.8 mm × 304.8 mm chamber maintained 1% error for 207 mm z-height, and 5% error for 255 mm z-height.

4. Experimental validation

To validate the design concept, the authors created a physical prototype of the inverted printer. This section describes experimental

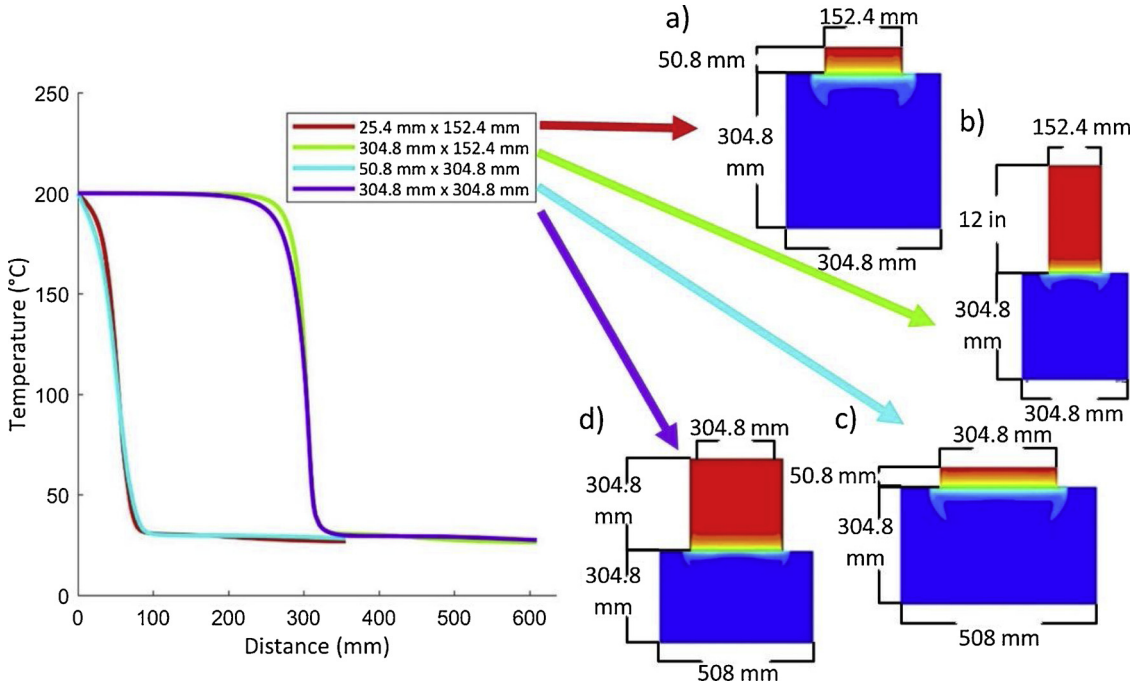

Fig. 5. The temperature profile of different sized heat chamber using a 2D Fluent model.

validation of the thermal model and evaluation of printed polyphenylsulfone (PPSF) parts. It was designed to match the temperature profiles of the simulation. The temperature of the chamber walls is controlled by two PID controllers (one mounted on the inverted bed and one the cylindrical wall) to control and maintain an isothermal boundary of 200 °C. After the temperatures stabilized, temperature measurements were taken with a K-type thermocouple at different distances from the bed. Measurements were taken at 25.4 mm increments from the print bed. All measurements were recorded as the average temperature over one minute. Following this validation, PPSF parts were then printed in the inverted build chamber to demonstrate the potential advantage of the system.

4.1. Method

4.1.1. Materials

The prototype for the 50.8 mm x 152.4 mm heat chamber consisted of an aluminum shell surrounded by heating elements and insulation. The total cost of the materials for the high temperature upgrade for an existing delta-style printer was less than $300.

Off the shelf PPSF-PPSU (1.75 mm diameter) filament from Stratasys was used for printing trials. This material has a reported glass transition temperature of 230 °C and heat deflection temperature of 189 °C [38]. Stratasys operating manual states a maximum extrusion temperature of 415 °C and a maximum oven temperature of 225 °C for printing PPSF in the Fortus system [39].

4.1.2. Printer design

The printer design was prototyped and tested using a custom delta robot 3D printer that features inverted control arms, as seen in Fig. 6. The system is controlled with an Arduino ATmega2560 running a custom version of Marlin firmware. The heated build chamber is located on the top of the printer, and features thick insulation (~25.4 mm alumina silica fiber insulation sheet and fiberglass fabric strips with plain backing from McMaster) and heaters on both the bed (Strip Heater without Temperature Control, 120 V AC, 120 W from McMaster) and walls of the chamber (Extreme-Temperature Heat Cable, 120 V AC, 468 W). An E3D V-6 print head was used with the PT100 thermocouple and a custom direct-drive extruder.

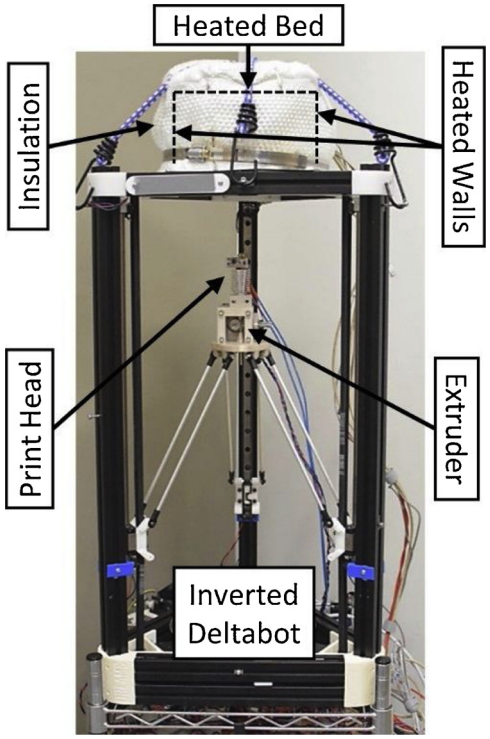

Fig. 6. Functional prototype of a custom delta printer modified with the inverted heated build chamber.

4.1.3. Tensile test

To compare the effect of printing PPSF in the inverted heated chamber, tensile specimens were printed at both an elevated temperature (200 °C) and room temperature (25 – 50 °C). The control "room temperature" printing trials had some temperature variation due to the print head heating the insulated print area. All other process parameters were kept constant between the builds to determine the effectiveness of the heated chamber independent of inversion and printing parameters. The infill was set to 95 % density with one perimeter and a rectilinear infill at +45°/-45° at 15 mm/s and a 0.2 mm layer height. Extrusion was done using a 0.4 mm nozzle at 350 °C. The print parameters were chosen for functionality; there remains the opportunity to further optimize parameters for part quality in future work. Parts were printed onto a PEI sheet that was secured to the inverted printer bed using Kapton tape. Printed parts were immediately removed from the printer following completion and set aside until the part cooled, when they were removed from the PEI sheet.

ASTM D638 Type V dogbones were printed in the XY plane and pulled on an Instron 5984 with a 10 kN load cell at 5 mm/min as per ASTM D638 [40]. A minimum of 4 dogbones were tested for each condition. The strain was calculated based on the distance of the grips. The elastic modulus was taken in the linear region where the linear fit had an R^2 value of 0.99.

4.2. Results

4.2.1. Experimental validation of thermal model

Fig. 7 shows the inverted system's temperature profile from both the thermal model (lines) and the experimentation (markers) using the inverted system. There is a large drop in temperature around 50.8 mm from the print bed, corresponding to the height of the chamber wall. The average temperature was used for the experiment and was within 8 °C to the pseudo transient model for all points except the points at the boundary of the chamber (50.8 mm), where there was an average of 19 °C discrepancy. The large variation at the boundary is expected due to the high temperature gradient at the boundary, which greatly affects any inaccuracy in the experimental distance measurement, and the

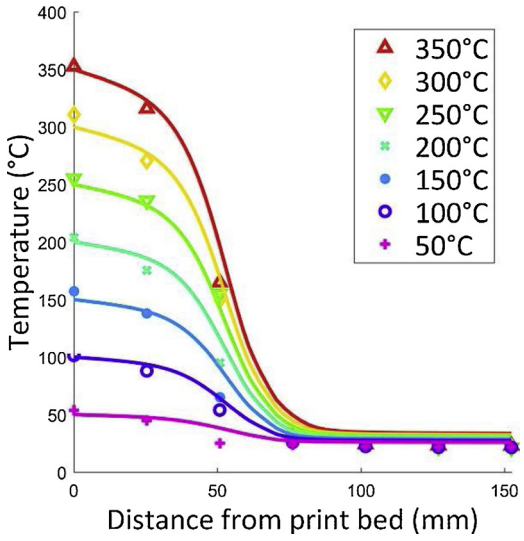

Fig. 7. Experimental and modeled temperatures from the center of the bed outward where the chamber bed and walls were set to 50-350 °C, in the inverted heat chamber. The markers represent the measured temperatures, while the line represents the temperature values from the simulation.

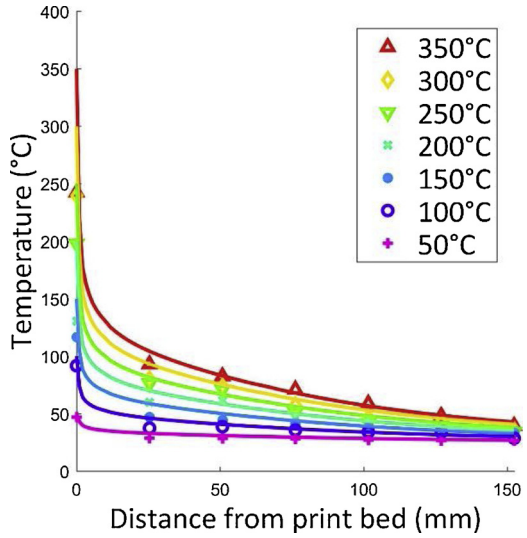

Fig. 8. The measured temperatures at different displacements from the bed at temperature controller set temperatures are between 50–350 °C, with a non-inverted heat chamber. The markers represent the experimental data, while the line represents the simulated data.

assumptions used to model the atmosphere.

The inverted build chamber was successfully heated to 400 °C measured at the heated bed. The authors expect that the temperature could be increased further even in this prototype build; however, 400 °C is greater than the melting temperature of most polymers and is likely sufficient for the build environment.

To validate the design decision to invert the print chamber, the results are compared to a traditional (non-inverted) chamber. An identical CFD simulation (Section 3) was performed with gravity inverted. The experimental data was collected with the chamber opening facing upwards. Fig. 8 presents a plot of the temperature profile for the non-inverted system. Heat is lost quickly using an open top heat chamber. The environmental temperature of the traditional system experiences an exponential decay at increasing distances from the print bed. Although the thermocouple used for the controller reached the set temperature (located on the underside of the print bed), the temperature on the top of the bed (where the part is printed) did not reach that temperature due to the loss in heat. The inverted heat chamber shows an asymptotic curve up to the set temperature, while the traditional design shows exponential decay to the room temperature. The dramatic loss in heat would be minimized if heated walls were not used, allowing heat to travel up through the center of the bed. However, at high temperatures, a printer with a heated bed and no heated walls still results in high energy loss and inconsistent heating.

4.2.2. Design validation via PPSF printing

PPSF Parts were printed on the inverted heated system to demonstrate the capability of high-temperature printing and to explore its impact on the resultant mechanical properties due to the heated environment. To explore the impact of the inverted heated build chamber, similar PPSF prints were completed on the same printer but without the heated chamber (i.e., parts were completed near room temperature). A sample of a printed tensile bars with and without the inverted heated build chamber can be seen in Fig. 9.

The tensile bars printed in the 200 °C chamber did not curl during printing. The room temperature environment tensile specimens curled as much as 2.34 mm the Z-direction, affecting the quality of the print, as well as the strength. The curling was so significant that a tensile bar (not used for tensile testing) fell off of the bed during the print, and the z-offset had to be adjusted to push the print head into the PEI sheet on the bed rather than being correctly calibrated.

The 200 °C environment temperature of the heated build environment prevents the material from shrinking during the print. The chamber temperature is below the glass transition temperature (230 °C) [38], so that the material is able to retain its shape. The authors believe the slight curvature in the ZY plane of the 200 °C specimen was caused during the part removal process from the PEI sheet or from a not optimized environment temperature.

Using PPSF's coefficient of thermal expansion provided by Stratasys [38], the room temperature tensile bars are calculated to shrink up to 0.6 mm more each layer in length (total 1.1 mm) than the high temperature tensile bars (0.5 mm) while cooling from the extrusion temperature to the environment temperature during printing. The discrete shrinkage of the bonded layers causes the residual stresses in the part to accumulate and cause the part to delaminate or curl. The material shrinks less while printing in the high-temperature environment, allowing the majority of the shrinking to occur after the part is printed and removed from the bed, where the part shrinks uniformly rather than discretely by layer.

Increasing the weld time between layers is critical to fabricating stronger bonds between roads and layer. Increasing the weld time increases the polymer chain diffusion across the interface and creates a stronger polymer weld [41]. Increasing the environment temperature decreases the rate of cooling, which increases the weld time. In addition, using a heated environment can allow for annealing of the part further increasing the part strength [15]. Heat treating a part after printing can increase the part strength, but requires additional processing time [11]. Using a high temperature heated environment allows for slower cooling during the print resulting in additional chain entanglement between the road and layer interfaces which increases the layer boning and the part strength, without a post-processing step.

Fig. 10 shows the compiled tensile data, where the elastic modulus between the two printing temperatures is within error and the ultimate tensile strength is 48 % higher for the higher environment temperature parts. The ultimate tensile strength for the PPSF specimens printed in the inverted high temperature environment was measured to be 62.62 ± 5.89 MPa, which is comparable to the reported strength (55 MPa) specified on the Stratasys PPSF data sheet for printing on a Fortus system [38]. The elastic modulus is not comparable to the Stratasys reported data, as the experimental procedure in this work measured effective strain (i.e., distance between the grips) and not true strain.

In order to qualitatively asses print quality, and to demonstrate the ability to print complex, solid geometries, the authors printed a PPSF 3D Benchy part in the high temperature environment (Fig. 11). 3D Benchy has been selected by the crowdsource community as a standard part for evaluating FFF printers' ability to print features including vertical and horizontal cylindrical holes, curved and flat overhangs, and high resolution details [42]. The part was printed at 15 mm/s using solid infill. All of the features were successfully printed with the inverted high temperature system, with the exception of the tiny surface detail (the 100 µm extrusion "#3DBenchy" nameplate), which is a detail that is difficult for most FFF systems. The authors attempted to print the same design in the room temperature environment, but it proved to be impossible as it failed early in the build by curling and falling off of the inverted bed during the first few layers. This part demonstrates that the high temperature design enables the printing of a complex structure.

5. Summary

Printing high-performance thermoplastics via FFF has proven challenging as the required high-temperature environments require expensive electronic components that have high operating temperatures. As such, currently commercially available high-temperature FFF systems cost > $30,000 and offer operating environments of less than 200 °C. In order to democratize the ability to 3D print high-performance

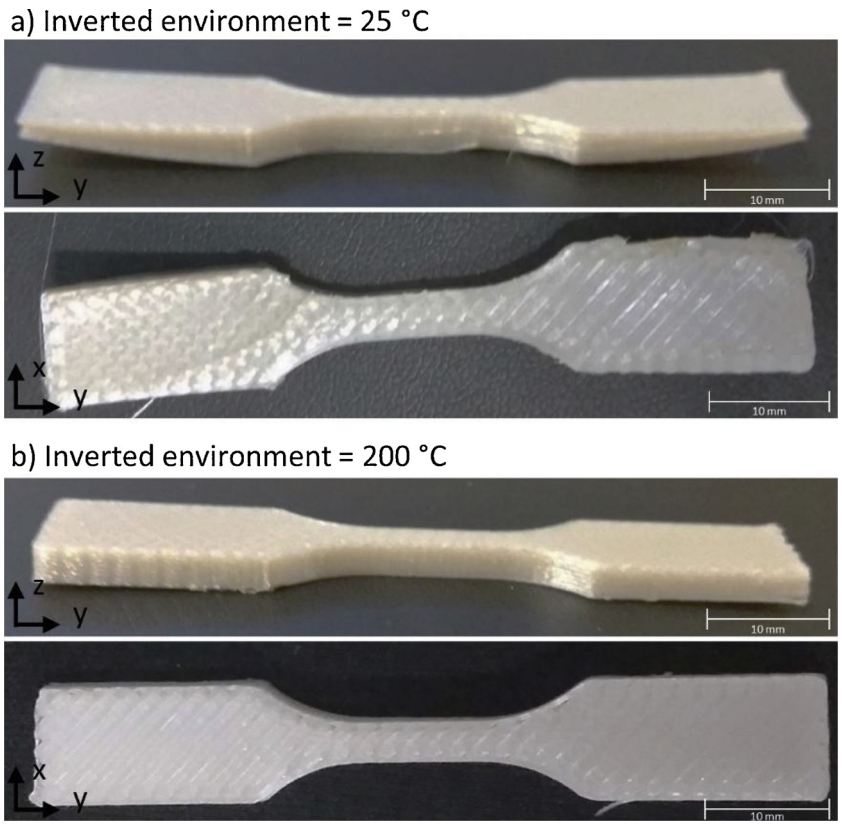

Fig. 9. Printed tensile bars using the inverted printer printed at 25 °C and 200 °C. The tensile bars are 63.5 mm in length, 9.53 mm in width, and 3.17 mm in height.

polymers by minimizing the cost of the FFF system, it is therefore critical to separate the electrical components from the high environment temperature. In this work, the authors have presented a novel approach for addressing this design trade-off by inverting the printer and printing inside of a heated chamber. The inverted heated chamber traps heat due to the difference in density between hot and cold air, while also allowing for full free movement of the print head. This design solution effectively separates the printer components from the high-temperature environment.

Both a computational fluid dynamics simulation and experimental measurements on a prototype systems demonstrated that an inverted chamber, with heated bed and walls, could be maintained at 200 °C for a 29.8 mm height with 5% error from the build plate in a 50.8 mm tall chamber. Tensile testing of PPSF specimens printed at 200 °C demonstrated a 48 % increase in the ultimate tensile strength compared to specimens printed at room temperature. The specimens printed in the ~$1000 inverted build chamber also demonstrated equivalent tensile properties to specimens printed on commercially available high-temperature FFF systems that retail for > $200,000. Complex structures with fine features and overhangs were also successfully printed with the inverted setup. This system can reach higher environment temperatures compared to machines in the current market and can be used to democratize manufacturing of high-performance polymers.

There is future work in creating a larger chamber to print larger

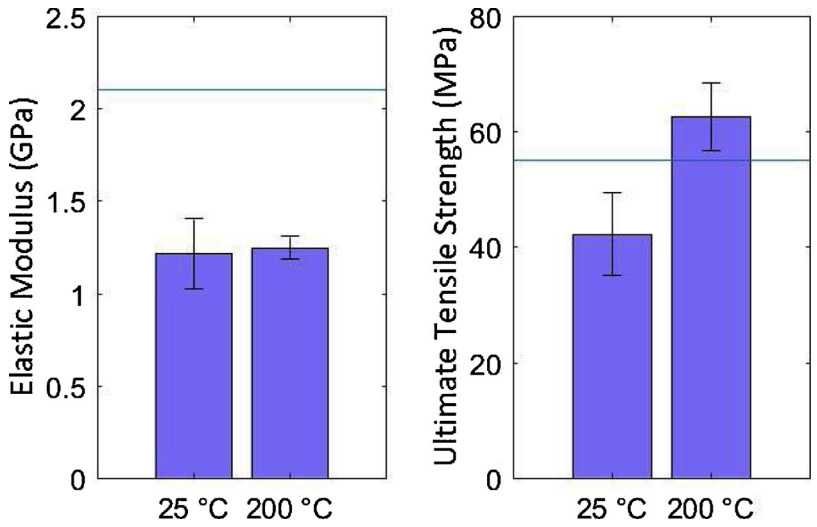

Fig. 10. Tensile properties of tensile bars printed on inverted FFF system at environment temperatures of 25 °C (n = 4) and 200 °C at 15 mm/s with a 200 µm layer height and 95 % rectilinear +45/−45 infill (n = 5). The horizontal line indicates reported Stratasys strength [38].

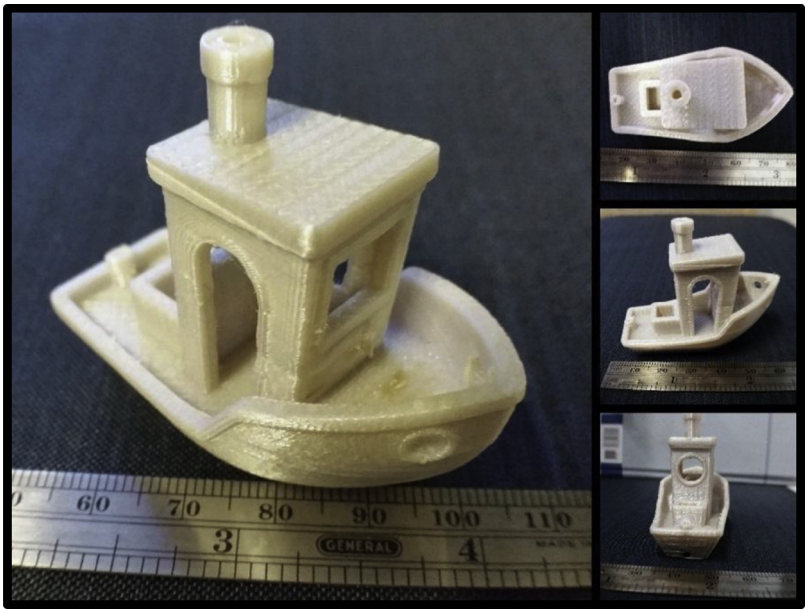

Fig. 11. A standard part (3D Benchy) was printed to demonstrate the ability to print more complex parts in the inverted high temperature system.

parts and limit the thermal gradient. Preliminary simulations indicate that the thermal gradient will remain at the boundary and a more stable environment temperature can be reached within a larger chamber. In addition, the thermal process simulation could be expanded to a three-dimensional model (instead of the presented 2D model) and include the effects of a moving heated print head to observe the impacts of air circulation distributed heat input (instead of the presented model's static extruder). While experimental results validated the current simulation, and the overall advantages of an inverted process chamber, such an updated model would improve the model's overall accuracy. Finally, the authors aim to explore the effects of gravity on the printed large parts in the inverted configuration.

CRediT authorship contribution statement

Callie Zawaski: Conceptualization, Methodology, Software, Validation, Investigation, Writing - original draft, Writing - review & editing, Visualization. **Christopher Williams:** Conceptualization, Writing - review & editing, Supervision, Project administration, Funding acquisition.

Declaration of Competing Interest

The authors declare that they have no known competing financial interests or personal relationships that could have appeared to influence the work reported in this paper.

Acknowledgements

The authors would like to acknowledge Jaideep Pandit for assistance and expertise with ANSYS Fluent, Tyler White for the previous work in drug delivery with the author that helped to inspire this design, Cam Chatham for polymer knowledge, Jake Fallon, Eric Gilmer, Cailean Pritchard, and Dr. Michael Bortner for high performance polymers knowledge. The authors acknowledge the Macromolecule Innovation Institute (MII) for inspiring and supporting interdisciplinary research and the Center for Enhancement of Engineering Diversity (CEED) for their financial support. This material is based upon work partially supported by the National Science Foundation under Grant No. 1254287 and 1934465.

References

[1] Wohlers Associates, Wohlers Report, (2019).
[2] K. Szykiedans, W. Credo, D. Osiński, Selected mechanical properties of PETG 3-D prints, Procedia Eng. 177 (2017) 455–461, https://doi.org/10.1016/j.proeng.2017.02.245.
[3] S.R.G. Bates, I.R. Farrow, R.S. Trask, 3D printed polyurethane honeycombs for repeated tailored energy absorption, Mater. Des. 112 (2016) 172–183, https://doi.org/10.1016/j.matdes.2016.08.062.
[4] A. Goyanes, A.B.M. Buanz, A.W. Basit, S. Gaisford, Fused-filament 3D printing (3DP) for fabrication of tablets, Int. J. Pharm. 476 (2014) 88–92, https://doi.org/10.1016/j.ijpharm.2014.09.044.
[5] D.W. Hutmacher, T. Schantz, I. Zein, K.W. Ng, S.H. Teoh, K.C. Tan, Mechanical properties and cell cultural response of polycaprolactone scaffolds designed and fabricated via fused deposition modeling, J. Biomed. Mater. Res. 55 (2001) 203–216, https://doi.org/10.1002/1097-4636(200105)55:2<203::AID-JBM1007>3.0.CO;2-7.
[6] F. Ning, W. Cong, J. Qiu, J. Wei, S. Wang, Additive manufacturing of carbon fiber reinforced thermoplastic composites using fused deposition modeling, Compos. Part B Eng. 80 (2015) 369–378, https://doi.org/10.1016/j.compositesb.2015.06.013.
[7] S.J. Leigh, R.J. Bradley, C.P. Purssell, D.R. Billson, D.A. Hutchins, A simple, low-cost conductive composite material for 3D printing of electronic sensors, PLoS One 7 (2012), https://doi.org/10.1371/journal.pone.0049365.
[8] J. Gonzalez-Gutierrez, S. Cano, S. Schuschnigg, C. Kukla, J. Sapkota, C. Holzer, Additive manufacturing of metallic and ceramic components by the material extrusion of highly-filled polymers: a review and future perspectives, Materials (Basel) 11 (2018), https://doi.org/10.3390/ma11050840.
[9] Y. Choi, C. Kim, H. Jeong, J. Youn, Influence of bed temperature on heat shrinkage shape error in FDM additive manufacturing of the ABS-engineering plastic, World J. Eng. Technol. 4 (2016) 186–192, https://doi.org/10.4236/wjet.2016.43D022.
[10] W. Swanson, P. Turley, P. Leavitt, P. Karwoski, J. LaBossiere, R. Skubie, High temperature modeling apparatus, US 6722872 B1, 2004. doi:10.1016/j.(73).
[11] C. Yang, X. Tian, D. Li, Y. Cao, F. Zhao, C. Shi, Influence of thermal processing conditions in 3D printing on the crystallinity and mechanical properties of PEEK material, J. Mater. Process. Technol. 248 (2017) 1–7, https://doi.org/10.1016/j.jmatprotec.2017.04.027.
[12] Y. Yan, R. Zhang, G. Hong, X. Yuan, Research on the bonding of material paths in melted extrusion modeling, Mater. Des. 21 (2000) 93–99, https://doi.org/10.1016/S0261-3069(99)00058-8.
[13] B.N. Turner, S.A. Gold, A review of melt extrusion additive manufacturing processes: II. Materials, dimensional accuracy, and surface roughness, Rapid Prototyp. J. 21 (2015) 250–261, https://doi.org/10.1108/RPJ-01-2013-0012.
[14] C. Duty, C. Ajinjeru, V. Kishore, B. Compton, N. Hmeidat, X. Chen, P. Liu, A.A. Hassen, J. Lindahl, V. Kunc, A viscoelastic model for evaluating extrusion-based print conditions, Solid Freeform Fabr. Symp. Proc. (2017) 495–506.
[15] W.J. Swanson, P.W. Turley, P.J. Leavitt, J. Karwoski, Peter, J.E. Labossiere, R.L. Skuble, High-temperature modeling method, US7,297,304 B2, 2007.
[16] P. Han, A. Tofangchi, A. Deshpande, S. Zhang, K. Hsu, An approach to improve interface healing in FFF-3D printed Ultem 1010 using laser pre-deposition heating, Procedia Manuf. 34 (2019) 672–677, https://doi.org/10.1016/j.promfg.2019.06.195.
[17] C. Sweeney, M. Green, M. Saed, Microwave-induce localized heating of CNT filled polymer composites for enhanced inter-bead diffusive bonding of fused filament

fabricated parts, US 2016/0325491, 2016.
[18] D. Ravoori, H. Prajapati, V. Talluru, A. Adnan, A. Jain, Nozzle-integrated pre-deposition and post-deposition heating of previously deposited layers in polymer extrusion based additive manufacturing, Addit. Manuf. 28 (2019) 719–726, https://doi.org/10.1016/j.addma.2019.06.006.
[19] J.E. Seppala, S. Hoon Han, K.E. Hillgartner, C.S. Davis, K.B. Migler, Weld formation during material extrusion additive manufacturing, Soft Matter 13 (2017) 6761–6769, https://doi.org/10.1039/C7SM00950J.
[20] B.N. Turner, R. Strong, S.A. Gold, A review of melt extrusion additive manufacturing processes: I. Process design and modeling, Rapid Prototyp. J. 20 (2014) 192–204, https://doi.org/10.1108/RPJ-01-2013-0012.
[21] L. Cherdo, 13 Professional PEEK 3D Printers (Also ULTEM®, PEI and High-Performance Materials), Aniwaa Pte. Ltd., 2018 (Accessed 2 August 2018), https://www.aniwaa.com/best-peek-3d-printer-pei-ultem/.
[22] Aon3D, Aon3D AON-M2, aon3d Inc., 2018 (Accessed 18 April 2018), https://www.aon3d.com/.
[23] Apium, Apium P220, Apium Addit. Technol. GmbH, 2018.
[24] INTAMSYS, INTAMSYS Funmat HT, INTAMSYS Technol. CO. LTD., 2017 (Accessed 1 August 2018), https://www.intamsys.com/.
[25] Oo-kuma, Oo-kuma Katana, (n.d.). http://www.oo-kuma.com/ (Accessed 1 August 2018).
[26] Roboz, Roboz One + 400, Web Agency BRAINPULL, 2018 (Accessed 1 August 2018), https://www.roboze.com/en/.
[27] Rokit, Rokit 3Dison AEP, www.3disonprinter.com. (n.d.). http://en.3disonprinter.com/index.php (Accessed 1 August 2018).
[28] Stratasys, Fortus 400mc, Strat. Ltd., 2018 (Accessed 1 August 2018), http://www.stratasys.com/.
[29] Tractus3D, Tractus3D T650P, Tractus3D, (2018) (Accessed 1 August 2018), https://tractus3d.com.
[30] VeraShape VSHAPER Pro, VSHAPER, VSHAPER, 2018 (Accessed 1 August 2018), http://vshaper.com/en/.
[31] I. Gibson, D. Rosen, B. Stucker, Additive Manufacturing Technologies 3D Printing, Rapid Prototyping, and Direct Digital Manufacturing, second edition, Springer, 2015, https://doi.org/10.1520/F2792-12A.2.
[32] H. Bheda, R. Reese, Fused Filament Fabrication using liquid cooling, US2016/0271880 A1, 2016. doi:10.1037/t24245-000.
[33] J.M. Gardner, C.J. Stelter, E.A. Yashin, E.J. Siochi, High Temperature Thermoplastic Additive Manufacturing Using Low-Cost, Open-Source Hardware, (2016), https://doi.org/10.13140/RG.2.2.20690.15049.
[34] R. Crockett, D. Petersen, K. Cooper, Fused deposition modeling in microgravity, Solid Freeform Fabr. Symp. Proc. (1999) 671–678.
[35] G. Wagner, L. Bass, D. Rau, S. Ziv, M. Wolf, D. Wolf, V. Meenakshisundaram, Y. Bai, C. Williams, Design and development of a multi-tool additive manufacturing system, Solid Freeform Fabr. Symp. Proc. (2017) 2005–2023.
[36] N.A. Meisel, A.M. Elliott, C.B. Williams, A procedure for creating actuated joints via embedding shape memory alloys in PolyJet 3D printing, J. Intell. Mater. Syst. Struct. 26 (2015) 1498–1512, https://doi.org/10.1177/1045389X14544144.
[37] C. Zawaski, E. Margaretta, A. Stevenson, A. Pekkaned, A. Whittington, T. Long, C.B. Williams, Embedding of liquids into water soluble materials via additive manufacturing for timed release, Solid Freeform Fabr. Symp. Proc. (2017) 2047–2059.
[38] Stratasys, PPSF Production-Grade Thermoplastic for Fortus 3D Printers, (2017).
[39] Stratasys, Fortus 360mc/400mc 3D Production System User Guide, (2014).
[40] G.P. Radar, E. Resistivity, D. Forensic, R. Methods, N. Ireland, ASTM D638: Standard Test Method for Tensile Properties of Plastics, (2015), https://doi.org/10.1520/C0186-15A.
[41] J. Seppala, K.E. Hillgartner, C.S. Davis, K. Migler, Thermography and weld strength characterization of thermoplastic 3D printing, SPE ANTE Indianap. (2016) 42–44.
[42] DBenchy, (2016) (Accessed 1 August 2018), http://www.3dbenchy.com/.